Oceanologia (2021) 63, 40—50

Available online at www.sciencedirect.com

ScienceDirect

journal homepage: www.journals.elsevier.com/oceanologia

ORIGINAL RESEARCH ARTICLE

# Satellite estimates of the long-term trend in phytoplankton size classes in the coastal waters of north-western Bay of Bengal

**Joereen Miranda[a,*], Aneesh Anandrao Lotliker[b], Sanjiba Kumar Baliarsingh[b], Amit Kumar Jena[a], Alakes Samanta[b], Kali Charan Sahu[a], Tummala Srinivasa Kumar[b]**

[a] *Department of Marine Sciences, Berhampur University, Bhanjabihar-760007, India*
[b] *Indian National Centre for Ocean Information Services, Ministry of Earth Sciences, Govt. of India, Hyderabad-500090, India*

Received 25 May 2020; accepted 11 September 2020
Available online 25 September 2020

**KEYWORDS**
MODISA;
Algorithm;
Coastal;
Monsoon;
Phytoplankton Size Classes

**Abstract** The study presents long-term variability in satellite retrieved phytoplankton size classes (PSC) at two coastal sites, off Gopalpur and Visakhapatnam, in the north-western Bay of Bengal. The abundance-based models by Brewin et al. (2010) (B10) and Sahay et al. (2017) (S17), for retrieval of PSC (micro, nano, and picophytoplankton), from satellite data, were validated. Both the models performed well in the retrieval of nano and microphytoplankton. However, B10 performed poorly in retrieving picophytoplankton. The statistical analysis indicated better performance of the S17 model and hence was applied to Moderate Resolution Imaging Spectroradiometer onboard Aqua satellite (MODISA) data to understand the temporal (at monthly climatology) and spatial variability (from nearshore to offshore). The spatial distribution indicated nearshore dominance of micro and offshore dominance of picophytoplankton. In nearshore waters off Gopalpur, microphytoplankton dominated throughout the year except for months of south-west monsoon (June and July) where the dominance of picophytoplankton was observed. All PSC exhibited similar distribution at an annual scale with a primary peak during pre-monsoon (March and April) and a secondary peak during post-monsoon (September—November). However, microphytoplankton concentration during post-monsoon was higher off Gopalpur in comparison to Visakhapatnam. The higher microphytoplankton concentration

* Corresponding author at: Department of Marine Sciences, Berhampur University, Bhanjabihar-760007, India.
*E-mail address:* joereen@gmail.com (J. Miranda).
Peer review under the responsibility of the Institute of Oceanology of the Polish Academy of Sciences.

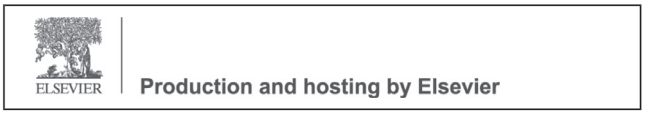


https://doi.org/10.1016/j.oceano.2020.09.003

during pre-monsoon was attributed to recurrent phytoplankton blooms. Whereas, post-monsoon increment could be attributed to enhanced phytoplankton growth by availing nutrients sourced from monsoonal precipitation induced terrigenous influx. The outcome of the present study recommends the use of the S17 model for satellite retrieval of PSC from the north-western Bay of Bengal.


## 1. Introduction

Phytoplankton are microscopic free-floating and/or drifting autotrophs present within the photic zone of the ocean and are major contributors to oceanic primary production (Uitz et al., 2010). Marine phytoplankton play a key character in the global carbon cycle and maintain the energy flow in the oceanic food web (Basu and Mackey, 2018). Apart from different taxonomic groups, phytoplankton, on the other hand, represent a range of size classes categorized as microphytoplankton (>20 μm), nanophytoplankton (<20 μm and >2 μm), and picophytoplankton (<2 μm and >0.2 μm) (Arin et al., 2002). The phytoplankton size classes (PSC) dwell in specific physico-chemical environments attributed to their nutrient uptake efficiency and cellular metabolism. In general, PSC play important role in marine biogeochemistry. Microphytoplankton (MP) are the particular size class photosynthetic group responsible for the substantial quantum of carbon export to the deep ocean and play an important role in sustaining fisheries (Murty et al., 2017). The transitional size class member, nanophytoplankton (NP) are represented by small flagellates belonging to several phytoplankton groups attributable to a higher amount of carbon fixation in oscillating environmental conditions (Hannah and Boney, 1983; Ribeiro et al., 2016). On the other hand, picophytoplankton (PP) are mostly comprised of cyanobacteria and prochlorophytes that prevail in oligotrophic waters due to high surface to volume ratio. Therefore, in the lower abundance condition of MP in oligotrophic offshore waters, PP carries out carbon recycling (Campbell and Vaulot, 1993; Campbell et al., 1994). The size distribution of the phytoplankton community has a significant influence on water quality (Baliarsingh et al., 2016, 2018). In turn, the variability pattern of physico-chemical parameters of the ecosystem also regulates the PSC distribution (Jyothibabu et al., 2015; Madhu et al., 2010).

The PSC distribution is generally depicted in terms of chlorophyll-*a* (chl-*a*) (Sahay et al., 2017). It is important to mention here that chl-*a*, the principal pigment of phytoplankton is broadly used as an index of phytoplankton biomass (Huot et al., 2007). Chl-*a* exhibits a specific spectral signature that enables its remote estimation using ocean colour remote sensing (IOCCG, 2000; Neil et al., 2019; O'Reilly et al., 1998). In the past decade, ocean colour remote sensing has been widely used for retrieval of chl-*a* from remote sensors. With the advancement in technology and novel bio-optical algorithms, PSC can be also retrieved from satellite data (Brewin et al., 2012, 2014). The discrete sampling of PSC lacks in providing information over a larger spatial area. This limitation can be overcome with satellite data having the capability to provide information at a synoptic scale with a high temporal resolution that can be used to study intra- and inter-annual variability of individual PSC (Sahay et al., 2017; Varunan and Shanmugam, 2015).

The north Indian Ocean comprises two essential components, the Arabian Sea and the Bay of Bengal (BoB). Although located at the same latitude, the processes controlling water quality largely differ in both the seas. The water quality variability in the BoB is largely controlled by the seasonally reversing monsoon currents, effluents discharge from perennial rivers and coastal industrial setups in addition to natural extreme events such as tropical cyclones. Several pockets of the north-western BoB experience recurrent algal blooms, eutrophication, and pollution. Studies on PSC distribution through *in situ*, as well as ocean colour sensors, are meagre in the coastal waters of the BoB.

The PSC forms an essential component of Phytoplankton Functional Types (PFT) in addition to taxonomy and pigment composition. The PFTs are of great interest to the biogeochemical community, especially in the coastal BoB, where the biological ecosystem is largely controlled by local and remote physical forcing (Lotliker et al., 2020; Miranda et al., 2020). The variability in PFTs can be directly linked to the phytoplankton efficiency in carbon sequestration and may be a function of climate change. On this backdrop, the present study aims to bridge the knowledge gap of PFT, in terms of PSC, with the objectives, (i) to evaluate two "abundance" based models for satellite estimation of PSC, and (ii) to understand the long-term trend of PSC at two ecologically important coastal sites, off Gopalpur and off Visakhapatnam, along the north-western BoB.

## 2. Material and methods

### 2.1. Study area

The BoB experiences various dynamic oceanographic processes such as seasonal reversal of wind, and current pattern along with immense freshwater discharge through rivers resulting in excess precipitation over evaporation (Varkey et al., 1996). The present study was carried out in the coastal waters off Gopalpur and off Visakhapatnam, north-western BoB (Figure 1). In general, waters along the coast of the eastern seaboard of India on north and south of 15°N are considered as north-western and south-western BoB, respectively (Lotliker et al., 2016). Both the study regions experience annual precipitation during the tropical south-west monsoon period from July to October bringing in adequate rainfall. However, the maximum rainfall is re-

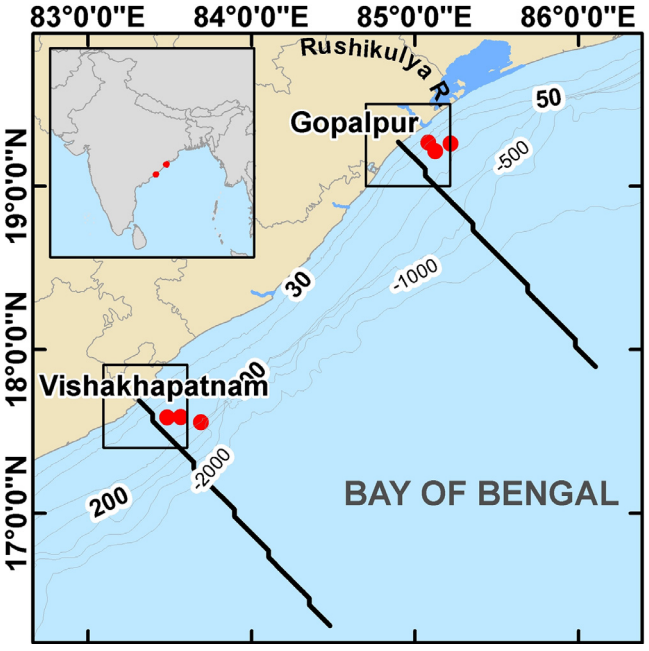


**Figure 1** Map of the study area. The dots indicate *in* situ sampling locations. The boxes represent areas of which time-series of satellite-derived size-fractionated chlorophyll-*a* (chl-*a*) were presented. The solid lines represent transects along which time-series of size-fractionated chl-*a* from satellite data is presented.

ceived from July to September during the active phase of the south-west monsoon season. The south-west monsoon gets totally withdrawn by October–November. During the north-east monsoon season, the BoB often experiences low pressure resulting in tropical cyclones. A significant amount of rainfall also occurs during this period. The north-east monsoon becomes inactive by end of November with the start of the winter season. The winter condition continues until February, after which the hot pre-monsoon conditions prevail spreading from March to May/June.

The circulation pattern of both regions is governed by more than one factor such as the effects of seasonally reversing East India Coastal Current (EICC) (Shetye et al., 1991), monsoonal wind-driven surface current (Vinayachandran and Mathew, 2003), cyclonic circulation (Vinayachandran and Yamagata, 1998) and river discharges flowing into the bay (Rao et al., 2007). The two major currents prevailing along this coast in a year are a north-easterly current that flows during January–July and a south-westerly current during August–December (Shankar et al., 2002). In addition, there are noticeable differences at both the locations on the local scale. The coastal waters off Gopalpur are well known for the periodic stay of migratory sea turtles, recurring high-biomass phytoplankton blooms and jellyfish swarming (Baliarsingh et al., 2016). The formation of two local water types on both sides of 30 m bathymetry makes coastal waters off Gopalpur ecologically distinct (Baliarsingh et al., 2015). The freshwater influx from the Rushikulya River estuary significantly influences the coastal water quality off Gopalpur. Additionally, upwelling along the coast, discharge from anthropogenic sources and sea-port activities also largely control biogeochemistry of the coastal waters off Gopalpur.

Visakhapatnam, (260 km south of Gopalpur), is a port city and receive no direct major river discharge into its coastal domain. However, a major river estuary (Godavari) is located ~200 km south of Visakhapatnam. The influx of Godavari estuary may have an impact on the coastal waters off Visakhapatnam during the south-west monsoon season due to high-flow condition (Shankar et al., 1996). The other minor rivers such as Gosthani and the Sarada-Varaha which are towards the north (15 km) and south (40 km), respectively of Visakhapatnam city have a meager impact on the coastal waters off Visakhapatnam during the non-monsoon season. However, coastal upwelling along with anthropogenic activities due to sea-port influences the biogeochemistry of Visakhapatnam coastal waters.

## 2.2. Methodology

### 2.2.1. In situ sampling and analysis

Seawater samples were collected onboard ORV *Sagar Manjusha* in four expeditions in the BoB during 2017 (May and October) and 2018 (July and November). During these expeditions, a total number of 18 samples for each PSC were collected within a distance of ~10 km from the coast. The water samples were collected using Niskin sampling bottles and a known volume was sequentially filtered through 20 μm (for MP), 2 μm (for NP) and 0.2 μm (for PP) pore size filter papers (Brewin et al., 2014). The filtration was carried out using a flow-through vacuum pump (make: Sartorius, model: Microstart Jet) under subdued light conditions. Subsequently, each filter was transferred to a sterilized cryotube and stored in liquid nitrogen until further analysis.

The chl-*a* concentration of individual PSC was estimated spectrophotometrically following the method prescribed by Parsons et al. (1984). The extraction of the pigment within the residue retained on the filter paper was carried out using 90% acetone. The extraction was carried out overnight with no light, under low temperature (in a refrigerator), and thereafter centrifuged for 20 minutes at 4000 rpm. The supernatant solution was then transferred to a 1 cm path length cuvette for analysis in a Double Beam UV-Visible Spectrophotometer (Make: Shimadzu, Model: UV-2600). The extinction coefficients of the sample were measured at specific wavelengths using acetone as blank. The chl-*a* concentration (in mg $m^{-3}$) was then calculated as follows (Strickland and Parsons., 1965).

$$\text{Chl-}a\left(\text{mg m}^{-3}\right) = \frac{[(11.6\times OD_{665})-(1.31\times OD_{645})-(0.14\times OD_{630})]\times v}{V\times l}$$

where OD is the optical density at discrete wavelengths after correction by the cell-to-cell blank and subtraction of the absorbance at 750 nm, *v* is volume of acetone in ml, *V* is the volume of filtered water in liter, and l is the path length in cm.

### 2.2.2. Satellite retrieval of size-fractionated chlorophyll-*a*

The daily Level-3 chl-*a* concentration from Moderate Resolution Imaging Spectroradiometer onboard Aqua satellite (MODISA) at 4 km resolution was acquired from National Aeronautics and Space Administration (NASA)'s Ocean Color Web supported by the Ocean Biology Processing

**Table 1** Model parameterization to calculate chlorophyll-*a* concentration in different size classes (pico, nano and microphytoplankton), using satellite data, provided by Brewin et al. (2010) and Sahay et al. (2017). The notations in the equations are chlorophyll-*a* concentration ($C$) which is the sum from pico ($C_P$), nano ($C_N$) and microphytoplankton ($C_M$). $C_{PN}^m$ and $C_P^m$ are the asymptotic maximum values that can be attained by the combination of pico- and nanophytoplankton ($C_{PN}$) and picophytoplankton ($C_P$), respectively. $S_{PN}$ and $S_P$ are the corresponding initial slopes.

$$C = C_P + C_N + C_M$$
$$C_{PN} = C_{PN}^m[1 - \exp(-S_{PN}C)]$$
$$C_M = C - C_{PN}$$
$$C_P = C_P^m[1 - \exp(-S_PC)]$$
$$C_N = C_{PN} - C_P$$

| Parameter | Brewin et al. (2010) | Sahay et al. (2017) |
|---|---|---|
| $C_{PN}^m$ | 0.977 | 1.2330 |
| $C_P^m$ | 0.095 | 0.7243 |
| $S_{PN}$ | 0.910 | 0.6792 |
| $S_P$ | 7.822 | 0.6645 |

Group (OBPG) (https://oceancolor.gsfc.nasa.gov/l3/). The abundance-based model of Brewin et al. (2010) (hereafter B10) and Sahay et al. (2017) (hereafter S17) were used to calculate chl-*a* concentration of each PSC. The B10 model is the extension of the approach of Satyendranath et al. (2001), whereas the S17 model is basically the B10 model tuned for the Arabian Sea. The mathematical formulations including the model parameters are provided in Table 1. These abundance-based models assume that the concentration of total chl-*a* (C) is the sum of the individual PSC fractions from PP ($C_P$), NP ($C_N$) and MP ($C_M$) (Brewin et al., 2010, 2012; Sahay et al., 2017).

$$C = C_P + C_N + C_M \quad (1)$$

The chl-*a* concentration of PP and the combined PP + NP fractions was parameterized as follows:

$$C_P = C_P^m[1 - \exp(-S_PC)] \quad (2)$$

$$C_{PN} = C_{PN}^m[1 - \exp(-S_{PN}C)] \quad (3)$$

where $C_P^m$ and $C_{PN}^m$ are the asymptotic values of maximum chl-*a* concentration attained by the combination of pico and nanophytoplankton ($C_{PN}$) and picophytoplankton ($C_P$). $S_{PN}$ and $S_P$ are the corresponding slopes. The chl-*a* concentration of MP and NP were subsequently calculated as follows:

$$C_M = C - C_{PN} \quad (4)$$

$$C_N = C_{PN} - C_P \quad (5)$$

The sensor-default atmospheric correction scheme was applied while generating chl-*a* from MODISA. The default, ocean chl-*a* with 3-band maximum ratio (OC3M) bio-optical algorithm was used for estimation of chl-*a* from MODISA. The functional form of the algorithm is expressed below.

$$\log_{10}(chl\text{-}a) = a_0 + \sum_{i=1}^{i=4} a_i \left\{ \log_{10}\left[ \frac{R_{rs}(\lambda_{blue})}{R_{rs}(\lambda_{green})} \right] \right\}^i \quad (6)$$

$$a = [0.2424,\ -2.7423,\ 1.8017,\ 0.0015,\ -1.2280] \quad (7)$$

For MODISA, $R_{rs}(\lambda_{blue})$ is the maximum of remote sensing reflectance ($R_{rs}$) at wavelengths ($\lambda$) 443 and 488 nm. $\lambda_{green}$ is 547 nm.

In addition, the monthly climatology of PSC was constructed for the period from 2002–2018. The monthly climatology was then averaged over a region of 0.5° × 0.5° off Gopalpur (19.0–19.5°N and 84.7–85.2°E), and off Visakhapatnam (17.4–17.9°N and 83.1–83.6°E) for subsequent assessment. In addition, the fractions of chl-*a* concentration of PP, NP and MP to total chl-*a* concentration were computed along the transect off Gopalpur and off Visakhapatnam from nearshore to 200 km offshore.

## 3. Results and discussion

### 3.1. Model performance in satellite retrieval of PSC

The satellite estimates of PSC have an advantage over conventional *in situ* data as they provide information over large spatial domains. Such information is necessary to discern ecosystem dynamics at the basin scale. However, the assessment of model accuracy in the retrieval of PSC from satellite data is also very important. Therefore, two "abundance" models B10 and S17 were applied to MODISA data and validated with *in situ* data generated within the study area. The satellite data were extracted within a box of 3 × 3 pixels, corresponding to *in situ* observations and the matchup points were selected containing more than 50% of the valid data (Bailey and Werdell, 2006). In addition to the concentration of chl-*a*, the fraction of individual PSC to total chl-*a* was also validated. The fraction depicts the contribution of individual PSC to the total concentration to represent and to understand the spatio-temporal trend (Brewin et al., 2015; Devred et al., 2011; Sahay et al., 2017). In the present study, fractions of individual PSC to total chl-*a* were used to understand the long-term trend from nearshore to offshore waters. Therefore, the fractions were also validated along with the concentrations of individual PSC.

**Table 2** Performance of statistical indices for the relative errors between *in situ* measured and satellite estimated chlorophyll-*a* (chl-*a*) concentration (mg $m^{-3}$) in various size classes (P: Pico, N: Nano and M: Microphytoplankton) and their fractions (%) to total chl-*a* concentration (F_P: Pico, F_N: Nano and F_M: Micro-phytoplankton) using Brewin et al. (2010) and Sahay et al. (2017) algorithms. Statistical indices include slope (S), intercept (I), regression coefficient ($R^2$), the average ratio of *in situ* measured to satellite estimated value (r), root mean squared error (RMSE) and the relative percentage difference between *in situ* measured and satellite estimated value (RPD). A total of 13 data points were used for validation.

| | | S | I | $R^2$ | r | RMSE | RPD |
|---|---|---|---|---|---|---|---|
| Brewin et al. (2010) | P | 25.08 | −1.99 | 0.51 | 0.32 | 0.28 | −262 |
| B10 | N | 0.45 | 0.05 | 0.72 | 1.81 | 0.23 | 40.2 |
| | M | 0.96 | 0.02 | 0.93 | 1.01 | 0.13 | −12.6 |
| | F_P | 0.65 | 26.35 | 0.60 | 0.36 | 22.28 | −235 |
| | F_N | 0.52 | 1.19 | 0.50 | 1.87 | 21.88 | 45.7 |
| | F_M | 0.77 | 8.81 | 0.83 | 1.00 | 5.21 | −1.6 |
| Sahay et al. (2017) | P | 0.82 | 0.07 | 0.77 | 0.98 | 0.07 | −7.8 |
| S17 | N | 0.90 | 0.03 | 0.74 | 0.99 | 0.05 | −7.7 |
| | M | 1.05 | 0.01 | 0.93 | 0.98 | 0.14 | −15.5 |
| | F_P | 0.97 | 0.28 | 0.72 | 1.03 | 3.60 | 2.0 |
| | F_N | 0.89 | 2.24 | 0.78 | 1.03 | 2.28 | 2.6 |
| | F_M | 0.93 | 3.95 | 0.83 | 0.97 | 4.63 | −4.4 |

The coastal areas of the north-western BoB often remain cloudy and a total of 13 match-up points were available. The *in situ* chl-*a* concentration of PP, NP and MP varied from 0.1 to 0.76, 0.07 to 0.87 and 0.05 to 2.88 mg $m^{-3}$, respectively which covers the entire dynamic range in the north Indian Ocean (Jyothibabu et al., 2013; Sarma et al., 2016; Sahay et al., 2017). Therefore, the *in situ* data was presented along with the dynamic range of the satellite estimates, using B10 (Figure 2a–c) and S17 (Figure 3a–c) model, for the corresponding months. The MODISA estimates of PSC are represented as minimum and maximum values over a month covering *in situ* sampling date. In addition, the relationship between *in situ* measured and satellite estimates of chl-*a* concentration in various size classes along with their fractions were also validated using B10 (Figure 2d–f) and S17 (Figure 3d–f) model. The statistical indices for the relative errors between *in situ* measured and MODISA estimates of PSC and their fractions (%) to total chl-*a* concentration are provided in Table 2.

The validation analysis showed underestimation and overestimation of the B10 model in retrieving PP (Figure 2a) and NP (Figure 2b), respectively. The statistical indicators also showed a high slope (25) and intercept (−1.99) for PP. The poor performance of the B10 model in capturing the *in situ* trend for PP is clearly evident with a low correlation coefficient ($R^2$=0.51). The statistical indicators for NP retrieval, using the B10 model showed low slope (0.45), low intercept (0.05) and good correlation ($R^2$=0.72). The B10 model performed well in estimating MP with all the *in situ* data falling within the dynamic range of MODISA (Figure 2c) with better slope (0.96), lower intercept (0.02), and good correlation ($R^2$=0.93). The estimated relative error in the retrieval of PSC from MODISA satellite data, using B10 model, was 262% for PP, 40.2% for NP and 12.6% for MP.

The S17 model performed relatively better, in comparison to B10. The *in situ* data falls well within the dynamic range of MODISA retrieved PP (Figure 3a), NP (Figure 3b) and MP (Figure 3c). The statistical indices for S17 showed better slope (0.82 to 1.05), lower intercept ($\leq$ 0.01), a good correlation coefficient ($R^2 \geq$ 0.74) and lower root mean squared error (RMSE) ($\leq$ 0.14). In addition, the estimated error in the retrieval of PSC from MODISA satellite data, using the S17 model, was 7.8% for PP, 7.7% for NP, and 15.5% for MP.

The fraction of PSC to total chl-*a* concentration was also statistically evaluated. The statistical performance indicators are provided in Table 2. The B10 model was found to be underestimating fractions of PSC with a slope value of $\leq$ 0.77. In addition, the fraction of PP and NP showed higher RMSE ($\geq$ 21.88), lower correlation coefficient ($R^2 \leq$ 0.6) and estimated error was 235 and 45.7%, respectively. However, the fraction of MP from the B10 model showed good performance with a slope value of 0.77, lower intercept (8.81), lower RMSE (5.21) and a high correlation coefficient ($R^2$=0.83). The estimated error was also lower (1.6%).

The S17 model performed much better in the retrieval of PSC fractions with a slope close to unity ($\geq$ 0.89), low intercept ($\leq$ 3.95), low RMSE ($\leq$4.63), high correlation (R2$\geq$0.72) and lower estimated error ($\leq$ 4.4%). The overall statistical results of PSC fraction was similar to that of absolute concentration where the poor performance of the B10 was observed to estimate the fraction of PP and NP. Considering the better performance, the subsequent analysis was carried out using the S17 model.

The estimation of PSC was carried out by using a three-component abundance model that calculates the fractional contribution from three PSC (PP, NP, and MP) to total chl-*a* concentration. The B10 model was the extension of the approach of Satyendranath et al. (2001), which was based on the assumption that the smaller cells dominate at lower chl-*a* concentrations and large cells at higher chl-*a* concentrations. In addition, the parameterization of the B10 model was carried out using *in situ* data from the Atlantic Ocean during the Atlantic Meridional Transect (AMT) campaign (Brewin et al., 2010). The B10 model performed well at a global scale when applied to Sea-Viewing Wide Field-of-View Sensor (SeaWiFS) data. Although the model was de-

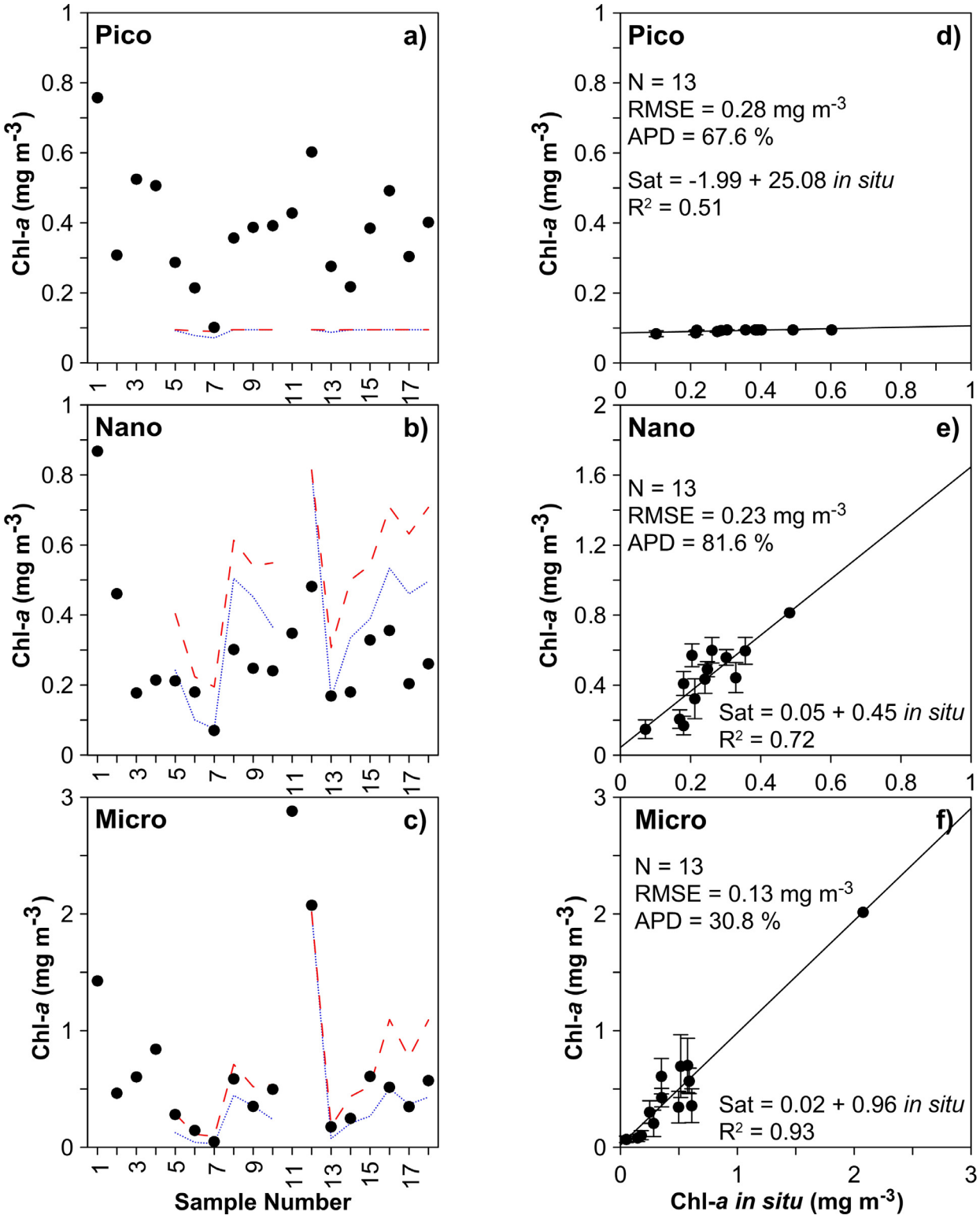


**Figure 2** The left panel represents variability between *in situ* measured (black dots) and satellite estimated (Brewin et al. 2010) chlorophyll-*a* (chl-*a*) concentration of a) pico, b) nano and c) microphytoplankton. The dotted (blue) line represents the minimum and dashed (red) line represents maximum value from satellite data over a month covering *in situ* sampling date. The right panel represents scatter plot showing relationship between *in situ* measured and satellite estimated (Brewin et al. 2010) chl-*a* concentration of d) pico, e) nano and f) microphytoplankton. The vertical bars indicate the standard deviation within *in situ* data.

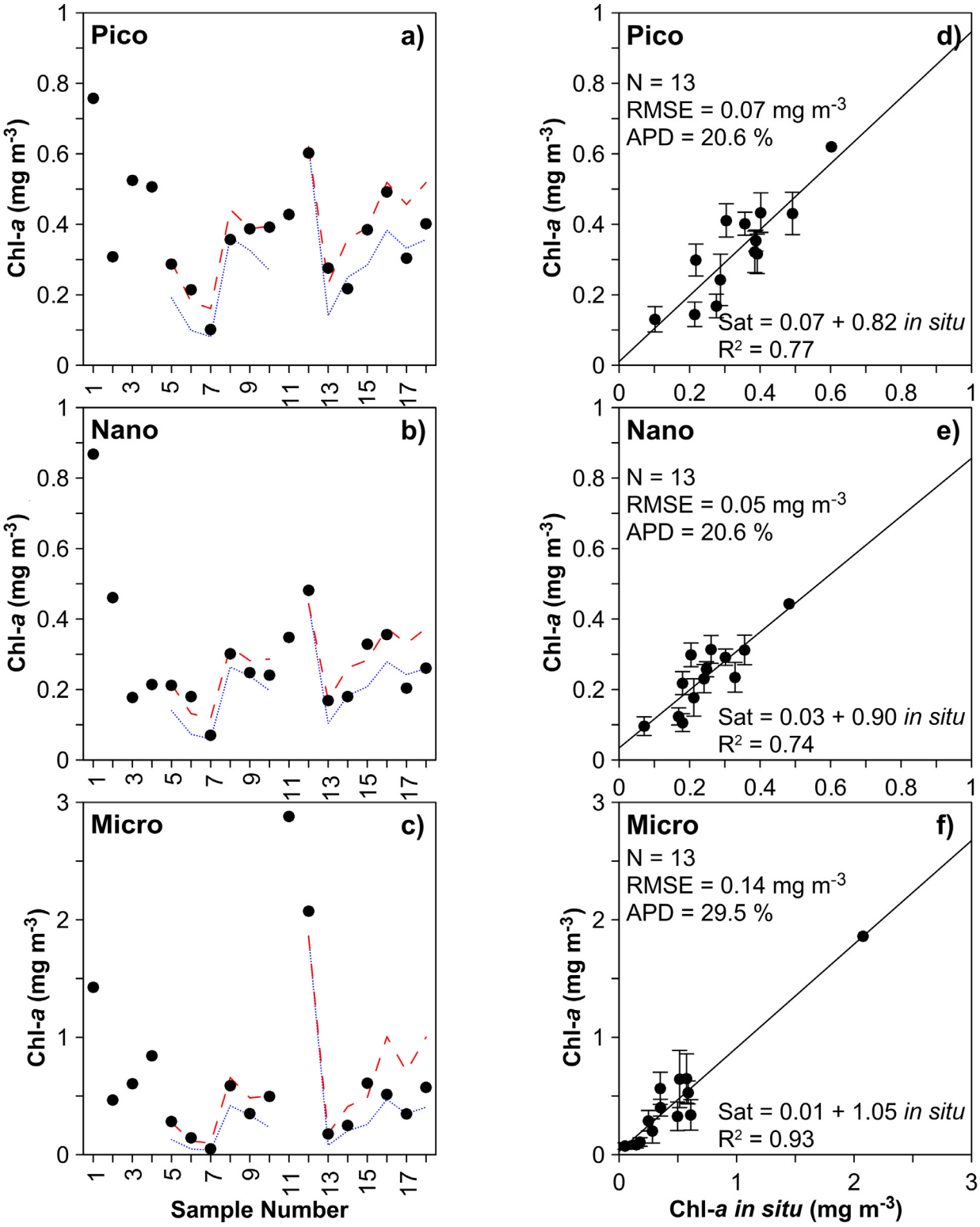


**Figure 3** The left panel represents variability between *in situ* measured (black dots) and satellite estimated (Sahay et al. 2017) chlorophyll-*a* (chl-*a*) concentration of a) pico, b) nano and c) microphytoplankton. The dotted (blue) line represents the minimum and dashed (red) line represents maximum value estimated from satellite data over a month covering *in situ* sampling date. The right panel represents scatter plot showing relationship between *in situ* measured and satellite estimated (Sahay et al. 2017) chl-*a* concentration of d) pico, e) nano and f) microphytoplankton. The vertical bars indicate the standard deviation within in situ data.

veloped for global application, the parameterization may vary with different biogeochemical provinces (Devred et al., 2009). In contrast, the S17 model is the regionally tuned version of Brewin et al. (2010) for the north Indian Ocean. The S17 model was tuned utilizing the *in situ* data from various Indian expeditions in the Arabian Sea including TARA Ocean Expedition dataset available in SeaWiFS Bio-optical Archive and Storage System (SeaBASS) maintained by the NASA — OBPG. The better performance of the S17 model could be attributed very well to its regional parameterization.

### 3.2. Long-term spatio-temporal distribution of PSC

The PSC are closely linked with several biogeochemical processes that have significant forcing on the marine carbon cycle, nutrient recycling and food web dynamics (Irwin et al., 2006). Therefore, the dynamics of PSC within the study area were analyzed through its spatial and temporal variability. The monthly climatology of PSC concentration and fractions was generated from MODISA data using S17 model. The monthly time-series of PSC averaged over 0.5° × 0.5° region off Gopalpur and Visakhapatnam is illustrated in Figure 4. The overall variability showed a similar trend with a peak during the pre-south-west monsoon (March—April) and the post-south-west monsoon (October) period. However, there was a marked difference in terms of the magnitude of individual PSC, especially during south-west monsoon and post south-west monsoon period. The distribution of PSC showed the dominance of MP throughout the year off Visakhapatnam (Figure 4b). However, PP dominated during south-west monsoon (June—July) and MP during rest of the year in coastal waters off Gopalpur. The cloudy condition and enhanced water column turbidity retards growth of large-sized phytoplankton in coastal waters and favours proliferation of small-sized phytoplankton during the monsoon season (Madhu et al., 2010). Further, the magnitude of all PSC was higher off Gopalpur during the post-south-west monsoon period (Figure 4a). The higher concentration during pre-monsoon could be attributed to the recurrent phytoplankton bloom events (Baliarsingh et al., 2016; Miranda et al.,

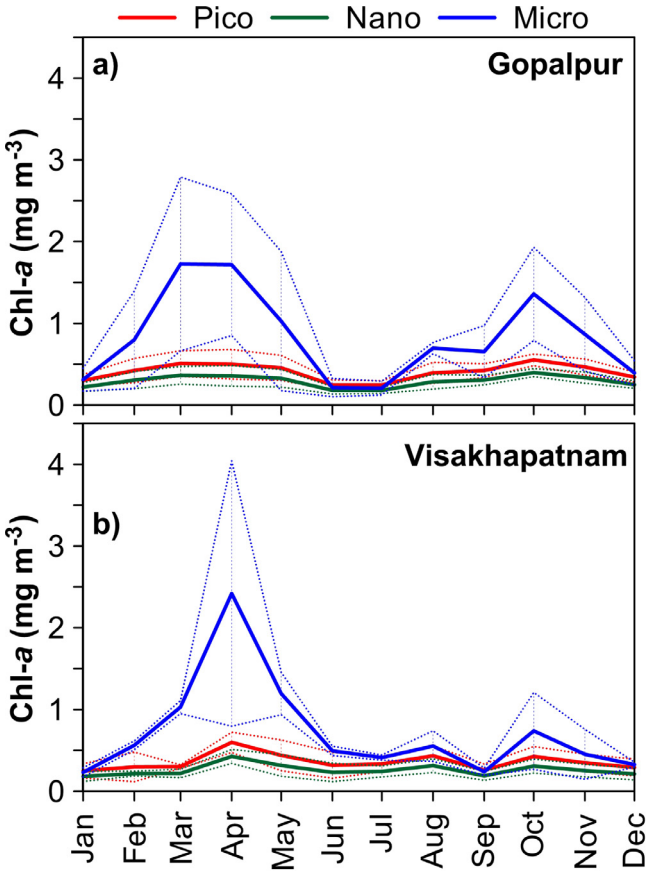


**Figure 4** Area averaged monthly climatolgical variability (2002—2018) of satellite estimated (Sahay et al., 2017) chlorophyll-*a* (chl-*a*) concentration of pico, nano and microphytoplankton in coastal waters of a) Gopalpur and b) Visakhapatnam. The area over which the average is taken is defined in Figure 1. The solid lines represent mean and dotted lines represent standard deviation.

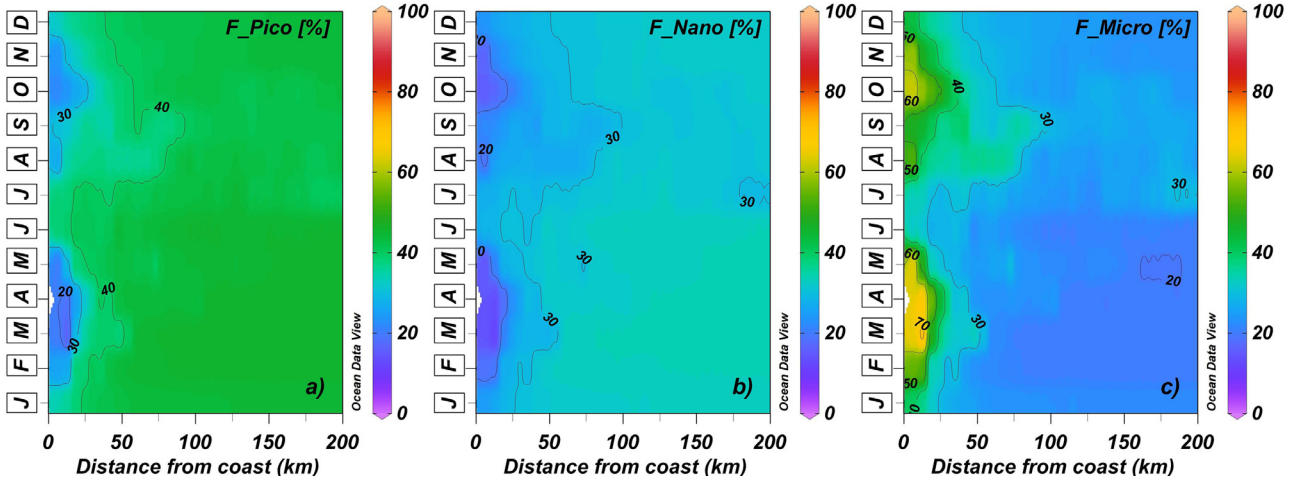


**Figure 5** Hovmöller diagram showing monthly climatological variability (2002—2018) in satellite estimated (Sahay et al., 2017) fractions of a) pico, b) nano and c) microphytoplankton concentration to total chlorophyll-*a* (chl-*a*) concentration along the transect (described in Figure 1) off Gopalpur.

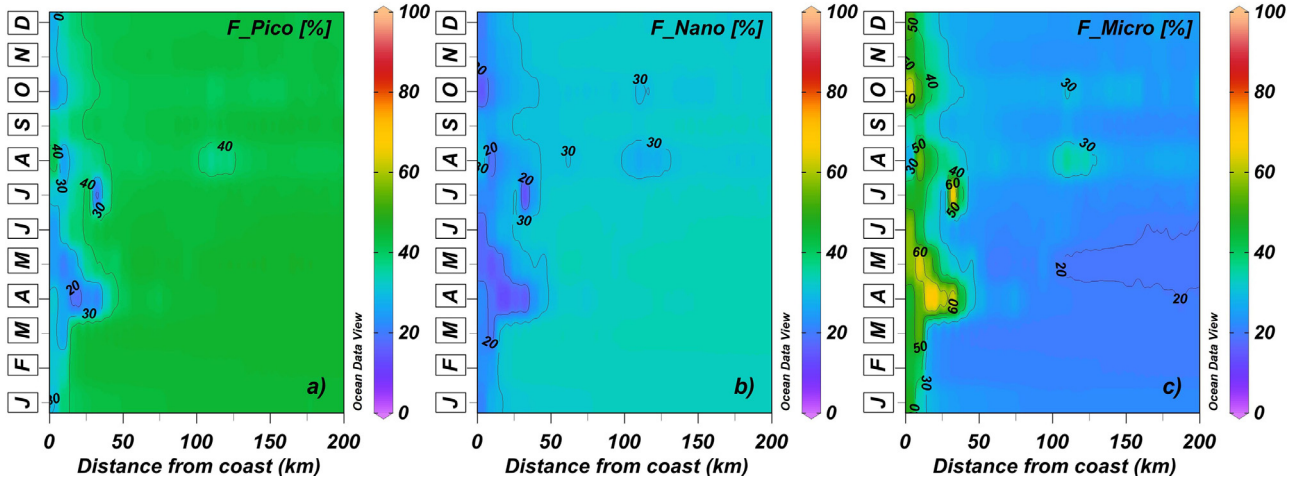


**Figure 6** Hovmöller diagram showing monthly climatological variability (2002—2018) in satellite estimated (Sahay et al., 2017) fractions of a) pico, b) nano and c) microphytoplankton concentration to total chlorophyll-*a* (chl-*a*) concentration along the transect (described in Figure 1) off Visakhapatnam.

2020). In general, the larger PSC prevails at higher concentrations of chl-*a*, whereas, both small, as well as large phytoplankton play an important role in the variability of chl-*a* at lower concentrations (Arin et al., 2005). The post-south-west monsoon increment could be attributed to enhanced phytoplankton growth by availing nutrients sourced from monsoonal precipitation induced terrigenous influx. The possible upwelling events enriching nutrients in the euphotic zone along the western BoB during the south-west monsoon season could also have played a pivotal role in elevating chl-*a* concentration (Rao et al., 1986; Shankar et al., 2002).

In subsequent analysis, nearshore to offshore variability in the fraction of PSC, off Gopalpur and Visakhapatnam, was analyzed through Hovmöller diagram (Figures 5 and 6). The nearshore dominance of MP and offshore dominance of PP were evident in both the areas. In nearshore region (up to 25 km from the coast), MP composition was nearly 70% that gradually decreased offshore in both the areas during the pre-south-west monsoon. During the post-south-west monsoon, up to 40% dominance of MP was observed off Gopalpur at a distance of ~4 km from the coast (Figure 5). However, the Visakhapatnam region showed less than 20% MP at a distance of ~40 km from the coast (Figure 6). In addition, during the south-west monsoon, nearshore waters off Gopalpur were observed with 40% of PP, 25% of NP and 35% of MP, whereas in off Visakhapatnam, PP, NP, and MP was 30%, 30% and 40%, respectively.

In corroboration to the present study, Mitbavkar and Anil (2011) have observed a higher abundance of PP in the offshore region of the BoB. In the open ocean region of the BoB, the PSCs percentage contribution to total chl-*a* have been reported in the order of PP > NP > MP. The higher contribution of PP was attributed to the low nutrient levels and a deeper nitracline (Sarma et al., 2016). The offshore higher abundance of PP in the BoB was comparatively higher than in the western counterpart, the Arabian Sea. Previous studies have reported ~30% and 70—80% contribution of PP to the total phytoplankton biomass in the Arabian Sea and the BoB, respectively (Baliarsingh et al., 2018; Mitbavkar and Anil, 2011; Roy et al., 2006). As a function of size, PP is capable of maintaining high uptake rates at low nutrient conditions, which gives a better competitive advantage over other PSCs in oligotrophic regions (Donald et al., 1997). In addition, PP also confers a greater efficiency to absorb and use solar radiation compared to larger PSC (Agusti et al., 1994).

## 4. Conclusions

Marine phytoplankton play a critical role in modulating the earth's climate and responsible for half of the planetary primary production. The phytoplankton biochemical functions such as nutrient uptake and growth rate are largely controlled by its size characteristics. In addition, absorption of light, photosynthetic rate, export production and the structure of the marine food chain depend upon phytoplankton size structure. The present study investigated the performance of two "abundance" based models for satellite estimation of PSC and to understand the long-term trend of PSC, using the best-suited model, at two ecologically important coastal sites, off Gopalpur and off Visakhapatnam, along the north-western BoB. This is the first attempt to study the long-term distribution of PSC using satellite data. The significant conclusions drawn from the present study are (i) better performance of three-component abundance-based S17 model in the estimation of PSC from the north-western BoB using MODISA satellite data, (ii) nearshore dominance of MP that gradually reduces offshore, (iii) dominance of MP throughout the year off Visakhapatnam, (iv) dominance of PP during south-west monsoon and MP rest of the year, respectively off Gopalpur, (v) possible source of higher MP concentration during pre-monsoon attributed to recurrent phytoplankton bloom, (vi) possible fuelling the post-south-west monsoon increment in MP concentration from monsoonal precipitation induced terrigenous influx enhancing phytoplankton growth. The present study recommends the use of S17 model for satellite retrieval of phytoplankton size classes from coastal waters of the north-western BoB. The satellite-based detection of PSC has provided a new avenue to study the spatio-temporal distribution that can be further linked to ocean climate dynamics. In addition, the

present study bridged the knowledge gap on PSC distribution in coastal waters of the north-western BoB.

## Acknowledgements

The authors wish to acknowledge NASA — GSFC for making available MODIS — Aqua data through OBPG project. The authors also thank the development team of SeaDAS, using which the satellite data was processed. The authors also acknowledge "Coastal Monitoring" programme of Indian National Centre for Ocean Information Services (INCOIS) for *in situ* data. The authors wish to acknowledge the encouragement and support extended by competent authorities of Berhampur University and INCOIS. This paper is part of the doctoral work of the first author (Joereen Miranda).

## References

Agusti, S., Enríquez, S., Frost-Christensen, H., Sand-Jensen, K., Duarte, C.M., 1994. Light harvesting among photosynthetic organisms. Funct. Ecol. 8, 273—279. https://doi.org/10.2307/2389911

Arin, L., Estrada, M., Salat, J., Cruzado, A., 2005. Spatio-temporal variability of size fractionated phytoplankton on the shelf adjacent to the Ebro river (NW Mediterranean). Cont. Shelf Res. 25 (9), 1081—1095. https://doi.org/10.1016/j.csr.2004.12.011

Arin, L., Morán, X.A.G., Estrada, M., 2002. Phytoplankton size distribution and growth rates in the Alboran Sea (SW Mediterranean): short term variability related to mesoscale hydrodynamics. J. Plankton Res. 24 (10), 1019—1033. https://doi.org/10.1093/plankt/24.10.1019

Bailey, S.W., Werdell, P.J., 2006. A multi-sensor approach for the on-orbit validation of ocean color satellite data products. Remote Sens. Environ. 102 (1—2), 12—23. https://doi.org/10.1016/j.rse.2006.01.015

Baliarsingh, S.K., Lotliker, A.A., Sahu, K.C., Kumar, T.S., 2015. Spatio-temporal distribution of chlorophyll-*a* in relation to physico-chemical parameters in coastal waters of the north-western Bay of Bengal. Environ. Monit. Assess. 187, art. no. 481. https://doi.org/10.1007/s10661-015-4660-x

Baliarsingh, S.K., Lotliker, A.A., Sudheesh, V., Samanta, A., Das, S., Vijayan, A.K., 2018. Response of phytoplankton community and size classes to green *Noctiluca* bloom in the northern Arabian Sea. Mar. Pollut. Bull. 129 (1), 222—230. https://doi.org/10.1016/j.marpolbul.2018.02.031

Baliarsingh, S.K., Lotliker, A.A., Trainer, V.L., Wells, M.L., Parida, C., Sahu, B.K., Srichandan, S., Sahoo, S., Sahu, K.C., Kumar, T.S., 2016. Environmental dynamics of red *Noctiluca scintillans* bloom in tropical coastal waters. Mar. Pollut. Bull. 111 (1—2), 277—286. https://doi.org/10.1016/j.marpolbul.2016.06.103

Basu, S., Mackey, K.R.M., 2018. Phytoplankton as key mediators of the biological carbon pump: Their responses to a changing climate. Sustainability 10 (3), 869. https://doi.org/10.3390/su10030869

Brewin, R.J.W., Sathyendranath, S., Jackson, T., Barlow, R., Brotas, V., Airs, R., Lamont, T., 2015. Influence of light in the mixed-layer on the parameters of a three-component model of phytoplankton size class. Remote Sens. Environ. 168, 437—450. https://doi.org/10.1016/j.rse.2015.07.004

Brewin, R.J.W., Hirata, T., Hardman-Mountford, N.J., Lavender, S.J., Sathyendranath, S., Barlow, R., 2012. The influence of the Indian Ocean Dipole on interannual variations in phytoplankton size structure as revealed by Earth Observation. Deep Sea Res. Pt. II 77—80, 117—127. https://doi.org/10.1016/j.dsr2.2012.04.009

Brewin, R.J.W., Sathyendranath, S., Hirata, T., Lavender, S.J., Barciela, R.M., Hardman-Mountford, N.J., 2010. A three-component model of phytoplankton size class for the Atlantic Ocean. Ecol. Model. 221 (11), 1472—1483. https://doi.org/10.1016/j.ecolmodel.2010.02.014

Brewin, R.J.W., Sathyendranath, S., Lange, P.K., Tilstone, G., 2014. Comparison of two methods to derive the size-structure of natural populations of phytoplankton. Deep Sea Res. Pt. I 85, 72—79. https://doi.org/10.1016/j.dsr.2013.11.007

Campbell, L., Nolla, H.A., Vaulot, D., 1994. The importance of *Prochlorococcus* to community structure in the central North Pacific Ocean. Limnol. Oceanogr. 39 (4), 954—961. https://doi.org/10.4319/lo.1994.39.4.0954

Campbell, L., Vaulot, D., 1993. Photosynthetic picoplankton community structure in the subtropical North Pacific Ocean near Hawaii (station ALOHA). Deep Sea Res Pt. I 40 (10), 2043—2060. https://doi.org/10.1016/0967-0637

Devred, E., Sathyendranath, E., Stuart, V., Platt, T., 2011. A three component classification of phytoplankton absorption spectra: Application to ocean-color data. Remote Sens. Environ. 115 (9), 2255—2266. https://doi.org/10.1016/j.rse.2011.04.025

Devred, E., Sathyendranath, S., Platt, T., 2009. Decadal changes in ecological provinces of the Northwest Atlantic Ocean revealed by satellite observations. Geophys. Res. Lett. 36 (19). art. no. L19607, https://doi.org/10.1029/2009GL039896

Donald, K.M., Scanlan, D.J., Carr, N.G., Mann, N.H., Joint, I., 1997. Comparative phosphorus nutrition of the marine cyanobacterium *Synechococcus* WH7803 and the marine diatom *Thalassiosira weissflogii*. J. Plankton Res. 19 (12), 1793—1813. https://doi.org/10.1093/plankt/19.12.1793

Hannah, F.J., Boney, A.D., 1983. Nanophytoplankton in the Firth of Clyde, Scotland: seasonal abundance, carbon fixation and species composition. J. Exp. Mar. Biol. Ecol. 67 (2), 105—147. https://doi.org/10.1016/0022-0981(83)90085-0

Huot, Y., Babin, M., Bruyant, F., Grob, C., Twardowski, M.S., Claustre, H., 2007. Does chlorophyll-*a* provide the best index of phytoplankton biomass for primary productivity studies? Biogeosciences Discuss. 4 (2), 707—745.

IOCCG, 2000. Remote sensing of ocean colour in coastal, and other optically-complex, waters. In: Sathyendranath, S. (Ed.), Reports of the International Ocean-Colour Coordinating Group, No. 3. IOCCG, Dartmouth, 1—140.

Irwin, A.J., Finkel, Z.V., Schofield, O.M.E., Falkowski, P.G., 2006. Scaling-up from nutrient physiology to the size-structure of phytoplankton communities. J. Plankton Res. 28 (5), 459—471. https://doi.org/10.1093/plankt/fbi148

Jyothibabu, R., Mohan, A.P., Jagadeesan, L., Anjusha, A., Muraleedharan, K.R., Lallu, K.R., Kiran, K., Ullas, N., 2013. Ecology and trophic preference of picoplankton and nanoplankton in the Gulf of Mannar and the Palk Bay, southeast coast of India. J. Marine Syst. 111—112, 29—44. https://doi.org/10.1016/j.jmarsys.2012.09.006

Jyothibabu, R., Vinayachandran, P.N., Madhu, N.V., Robin, R.S., Karnan, C., Jagadeesan, L., Anjusha, A., 2015. Phytoplankton size structure in the southern Bay of Bengal modified by the Summer Monsoon Current and associated eddies: Implications on the vertical biogenic flux. J. Marine Syst. 143, 98—119. https://doi.org/10.1016/j.jmarsys.2014.10.018

Lotliker, A.A., Baliarsingh, S.K., Sahu, K.C., Kumar, T.S., 2020. Long-term chlorophyll-*a* dynamics in tropical coastal waters of the western Bay of Bengal. Environ. Sci. Pollut. Res. 27, 6411—6419. https://doi.org/10.1007/s11356-019-07403-0

Lotliker, A.A., Omand, M.M., Lucas, A.J., Laney, S.R., Mahadevan, A., Ravichandran, M., 2016. Penetrative radiative flux in the Bay of Bengal. Oceanography 29 (2), 214—221. https://doi.org/10.5670/oceanog.2016.53

Madhu, N.V., Jyothibabu, R., Balachandran, K.K., 2010. Monsoon-induced changes in the size-fractionated phytoplankton biomass and production rate in the estuarine and coastal waters of southwest coast of India. Environ. Monit. Assess. 166, 521—528. https://doi.org/10.1007/s10661-009-1020-8

Miranda, J., Baliarsingh, S.K., Lotliker, A.A., Sahoo, S., Sahu, K.C., Kumar, T.S., 2020. Long-term trend and environmental determinants of phytoplankton biomass in coastal waters of northwestern Bay of Bengal. Environ. Monit. Assess. 192, 55. https://doi.org/10.1007/s10661-019-8033-8

Mitbavkar, S., Anil, A.C., 2011. Tiniest primary producers in the marine environment: an appraisal from the context of waters around India. Curr. Sci. 100 (7), 986—988.

Murty, K.N., Sarma, N.S., Pandi, S.R., Chiranjeevulu, G., Kiran, R., Muralikrishna, R., 2017. Hydrodynamic control of microphytoplankton bloom in a coastal sea. J. Earth Syst. Sci. 126, 82. https://doi.org/10.1007/s12040-017-0867-2

Neil, C., Spyrakos, E., Hunter, P.D., Tyler, A.N., 2019. A global approach for chlorophyll-*a* retrieval across optically complex inland waters based on optical water types. Remote Sens. Environ. 229, 159—178. https://doi.org/10.1016/j.rse.2019.04.027

O'Reilly, J.E., Maritorena, S., Mitchell, B.G., Siegel, D.A., Carder, K.L., Garver, S.A., Kahru, M., McClain, C., 1998. Ocean color chlorophyll algorithms for SeaWiFS. J. Geophys. Res.-Oceans 103 (C11), 24937—24953. https://doi.org/10.1029/98JC02160

Parsons, T.R., Maita, Y., Lalli, C.M., 1984. A Manual of Chemical and Biological Methods for Seawater Analysis. Pergamon Press, New York, 173 pp.

Rao, A.D., Dash, S., Jain, I., Dube, S.K., 2007. Effect of estuarine flow on ocean circulation using a coupled coastal-bay estuarine model: an application to the 1999 Orissa cyclone. Nat. Hazards 41, 549—562. https://doi.org/10.1007/s11069-006-9049-2

Rao, T.V.N., Rao, D.P., Rao, B.P., Raju, V.S.R., 1986. Upwelling and sinking along Visakhapatnam coast. Indian J. Mar. Sci. 15, 84—87.

Ribeiro, C.G., Santos, A.L., Marie, D., Pellizari, V.H., Brandini, F.P., Vaulot, D., 2016. Pico and nanoplankton abundance and carbon stocks along the Brazilian Bight. PeerJ.. 4, art. no. e2587, https://doi.org/10.7717/peerj.2587

Roy, R., Pratihary, A., Mangesh, G., Naqvi, S.W.A., 2006. Spatial variation of phytoplankton pigments along the southwest coast of India. Estuar. Coast Shelf Sci. 69 (1—2), 189—195. https://doi.org/10.1016/j.ecss.2006.04.006

Sahay, A., Ali, S.M., Gupta, A., Goes, J.I., 2017. Ocean color satellite determinations of phytoplankton size class in the Arabian Sea during the winter monsoon. Remote Sens. Environ. 198, 286—296. https://doi.org/10.1016/j.rse.2017.06.017

Sarma, V.V.S.S., Rao, G.D., Viswanadham, R., Sherin, C.K., Salisbury, J., Omand, M.M., Mahadevan, A., Murty, V.S.N., Shroyer, E.L., Baumgartner, M., Stafford, K.M., 2016. Effects of freshwater stratification on nutrients, dissolved oxygen, and phytoplankton in the Bay of Bengal. Oceanography 29 (2), 222—231. https://doi.org/10.5670/oceanog.2016.54

Sathyendranath, S., Cota, G., Stuart, V., Maass, H., Platt, T., 2001. Remote sensing of phytoplankton pigments: a comparison of empirical and theoretical approaches. Int. J. Remote Sens. 22 (2—3), 249—273. https://doi.org/10.1080/014311601449925

Shankar, D., McCreary, J.P., Han, W., Shetye, S.R., 1996. Dynamics of the East India Coastal Current: 1. Analytic solutions forced by interior Ekman pumping and local alongshore winds. J. Geophys. Res.-Oceans 101 (C6), 13975—13991. https://doi.org/10.1029/96JC00559

Shankar, D., Vinayachandran, P.N., Unnikrishnan, A.S., 2002. The monsoon currents in the north Indian Ocean. Prog. Oceanogr. 52 (1), 63—120. https://doi.org/10.1016/S0079-6611(02)00024-1

Shetye, S.R., Shenoi, S.S.C., Gouveia, A.D., Michael, G.S., Sundar, D., Nampoothiri, G., 1991. Wind-driven coastal upwelling along the western boundary of the Bay of Bengal during the southwest monsoon. Cont. Shelf Res. 11 (11), 1397—1408. https://doi.org/10.1016/0278-4343(91)90042-5

Strickland, J.D.H., Parsons, T.R., 1965. A manual of seawater analysis. Bull. 125. Fisher. Res. Board Can., Ottawa, 203 pp.

Uitz, J., Claustre, H., Gentili, B., Stramski, D., 2010. Phytoplankton class-specific primary production in the world's oceans: seasonal and interannual variability from satellite observations. Global Biogeochem. Cy. 24 (3). art. no. GB3016, https://doi.org/10.1029/2009GB003680

Varkey, M.J., Murthy, V.S.N., Suryanarayana, A., 1996. Physical oceanography of the Bay of Bengal and Andaman Sea. Oceanogr. Mar. Biol. Ann. Rev. 34, 1—70.

Varunan, T., Shanmugam, P., 2015. A model for estimating size-fractioned phytoplankton absorption coefficients in coastal and oceanic waters from satellite data. Remote Sens. Environ. 158, 235—254. https://doi.org/10.1016/j.rse.2014.11.008

Vinayachandran, P.N., Mathew, S., 2003. Phytoplankton bloom in the Bay of Bengal during the northeast monsoon and its intensification by cyclones. Geophys. Res. Lett. 30 (11). art. no. 1572, https://doi.org/10.1029/2002GL016717

Vinayachandran, P.N., Yamagata, T., 1998. Monsoon response of the sea around Sri Lanka: generation of thermal domes and anticyclonic vortices. J. Phys. Oceanogr. 28 (10), 1946—1960 https://doi.org/10.1175/1520-0485(1998)028⟨1946:MROTSA⟩2.0.CO;2